HAL
open science

Oxidation resistance of Ti 3 AlC 2 and Ti 3 Al 0.8 Sn 0.2 C 2 MAX phases: A comparison

Elodie Drouelle, Véronique Brunet, Jonathan Cormier, Patrick Villechaise, Pierre Sallot, Foad Naimi, Frederic Bernard, Sylvain Dubois

To cite this version:

Elodie Drouelle, Véronique Brunet, Jonathan Cormier, Patrick Villechaise, Pierre Sallot, et al.. Oxidation resistance of Ti 3 AlC 2 and Ti 3 Al 0.8 Sn 0.2 C 2 MAX phases: A comparison. Journal of the American Ceramic Society, 2019, 103 (2), pp.1270-1280. 10.1111/jace.16780 . hal-03100621

HAL Id: hal-03100621

https://hal.science/hal-03100621v1

Submitted on 6 Jan 2021

HAL is a multi-disciplinary open access archive for the deposit and dissemination of scientific research documents, whether they are published or not. The documents may come from teaching and research institutions in France or abroad, or from public or private research centers.

L'archive ouverte pluridisciplinaire **HAL**, est destinée au dépôt et à la diffusion de documents scientifiques de niveau recherche, publiés ou non, émanant des établissements d'enseignement et de recherche français ou étrangers, des laboratoires publics ou privés.

Oxidation resistance of Ti_3AlC_2 and $Ti_3Al_{0.8}Sn_{0.2}C_2$ MAX phases: a comparison

E. Drouelle[1,2], V. Brunet[1], J. Cormier[1], P. Villechaise[1], P. Sallot[2], F. Naimi[3], F. Bernard[3] and S. Dubois[1]

[1] Institut PPRIME, CNRS/Université de Poitiers/ENSMA, UPR 3346 CNRS, Boulevard M. et P. Curie, BP 30179, 86962 Chasseneuil du Poitou-Futuroscope Cedex, France

[2] Safran Tech, 1 rue Geneviève Aubé, CS 80112, 78772 Magny les hameaux Cedex, France

[3] Laboratoire Interdisciplinaire Carnot de Bourgogne, UMR 6303 CNRS-Université de Bourgogne Franche-Comté, 9 Av. Alain Savary, BP 47870, 21078 DIJON Cedex, France

Abstract

Ti_3AlC_2 and $Ti_3Al_{0.8}Sn_{0.2}C_2$ MAX phase powders are densified using Spark Plasma Sintering technique to obtain dense bulk materials. Oxidation tests are then performed over the temperature range 800-1000°C under synthetic air on the two different materials in order to compare their oxidation resistance. It is demonstrated that, in the case of the $Ti_3Al_{0.8}Sn_{0.2}C_2$ solid solution, the oxide layers consist in TiO_2, Al_2O_3 and SnO_2. The presence of Sn atoms in the A planes of the solid solution leads to an easy diffusion of Sn out of the MAX phase which promote the formation of the non-protective and fast growing SnO_2 oxide. Moreover, the small Al/Ti atom's ratio promotes the growth of a non-protective rutile-TiO_2 scale as well. In the case of the Ti_3AlC_2 MAX phase, the oxide layer consists in a protective alumina scale; a few TiO_2 grains being observed on the top of the Al_2O_3 layer. The parabolic oxidation rate constants are about 3 orders of magnitude smaller for Ti_3AlC_2 compared to $Ti_3Al_{0.8}Sn_{0.2}C_2$.

I – Introduction

MAX phases are a family of nanolaminated ternary nitrides and carbides, with the general formula $M_{n+1}AX_n$ (n=1 to 3), where M is a transition metal, A is an element from group A, and X is either carbon or nitrogen[1]. Depending on the n value, they are now often named 413 (n=3), 312 (n=2) or 211 (n=1) MAX phase. These compounds were first discovered in the 1960s[2-4], however, they were revived in 1995 when Barsoum *et al*. discovered that they exhibit unique physical and chemical properties[5]. The three compounds crystallize in a hexagonal P63/mmc lattice characterized by M_6X octahedra separated by A atomic layers. Their unique structure, combining both strong covalent M-X bonds and weaker M-A bonds, confers to MAX phases properties of both classes of materials. Like ceramics, they are stiff, lightweight, chemically stable and oxidation resistant. Like metals, they are relatively soft, machinable, resistant to thermal shock and they exhibit good electric and thermal conductivity as well as good damage tolerance[5-7].

Among the 312 phases, Ti_3AlC_2 and its solid solution have attractive properties. Ti_3AlC_2 possesses quite remarkable properties such as low density (4.25g/cm^3), high Young's modulus (297 GPa), high strength at high temperature, self-lubrication, good machinability, high thermal and electrical conductivity *etc*[8-10]. Moreover, Alumina-forming MAX phases are well-known for their excellent oxidation resistance[11-19b], rivaling many metallic NiAl, NiCrAl, and FeCrAl counterparts PhD thesis Elodie and with upper temperature capability possible to ~1400 °C. Hence, these remarkable properties make Ti_3AlC_2 a promising material for various applications. However, before they can be used it is imperative to be able to predict the oxide thicknesses that would form after long times at elevated temperatures. This, in turn implies that the oxidation kinetics be well understood and documented. Pietzka and Schuster first synthesized bulk polycrystalline Ti_3AlC_2 by sintering cold-compacted powder mixtures of Ti, TiAl, Al_4C_3 and C at 1573 K under pure hydrogen for 20h[20]. Tzenov and Barsoum prepared bulk

polycrystalline Ti_3AlC_2 (4 vol.% Al_2O_3 as impurity in the sample) by reactive Hot Isostatic Pressing (HIP) at 70MPa and 1400°C for 16h using a mixture of Ti, C and Al_4C_3 powders and investigated some properties of the as-synthesized samples[8]. Wang and Zhou produced fully dense Ti_3AlC_2 using a solid–liquid reaction synthesis and simultaneous in situ hot pressing process using a mixture of Ti, Al, and graphite as starting powders[21]. Zhou et al. fabricated Ti_3AlC_2 by Self-propagating High-temperature Synthesis (SHS) from elemental Ti, Al and C, followed by a densification step using the Spark-Plasma Sintering (SPS) method[22]. However, the purity of the Ti_3AlC_2 was not easy to control, because of the thermal explosion that occurred among the elemental raw materials. Zhu et al. synthesized Ti_3AlC_2 by hot pressing TiC, Ti, and Al powders at 1573–1673 K for 2 h under a pressure of 30 MPa[23]. Finally, a variety of methods are implemented to prepare Ti_3AlC_2 bulk samples or Ti_3AlC_2 powder samples. Nevertheless, it is difficult to obtain a single-phase Ti_3AlC_2 material due to the narrow phase domain in the Ti-Al-C phase diagram. Impurities such as TiC, Ti_xAl_y intermetallics, Al_2O_3 or the 211 MAX phase (Ti_2AlC) are commonly detected in the end-products[10,24-30]. Especially, the presence of TiC invariably deteriorates the high electrical conductivity[7], the oxidation resistance[18] and some other properties of Ti_3AlC_2. Thus, several sintering additives such as Si[31], Sn[32,33] and B_2O_3[34] were introduced into Ti-Al-C system to avoid impurity formation and to get the Ti_3AlC_2 single phase. The former research work by Ai *et al.*[32] and Li *et al.*[33] has proved that Sn is an efficient additive to inhibit the TiC impurity formation. A nearly pure Ti_3AlC_2 was thus obtained in a relative wide temperature range by pressureless sintering 3Ti+Al+1.8C with 0.2 mol of added Sn. Ai *et al.*[32] also detected some Sn in the final products by Energy Dispersive X-ray Spectrometry (EDXS) and reported more Sn distributed in the grain boundary rather than in the Ti_3AlC_2 structure. Bei et al. have studied, in details, the synthesis of $Ti_3Al_{1-x}Sn_xC_2$ solid solution by Hot Isostatic Pressing[33b,33c].

The first paper describing the oxidation behaviour of $Ti_{n+1}AlC_n$ has been published in 2001[14]. Since that date, the high-temperature oxidation behavior of Ti_3AlC_2 has been extensively studied[11-19c]; a review paper can also be found[15]. However, to our knowledge, the oxidation behaviour of $Ti_3Al_{(1-x)}Sn_xC_2$ solid solution has not been studied. Barsoum studied the oxidation behavior of Ti_3AlC_2 at 1073–1373 K in air for exposure times up to 100 h[8,14]. The oxide layers mainly consist in a rutile-based solid solution, $(Ti_{1-y}Al_y)O_{2-y/2}$ with $y < 0.05$, and some Al_2O_3. Barsoum's specimens formed thick and highly striated oxide layers during high-temperature oxidation. Barsoum further explained that the subjection of the $(Ti_{1-y}Al_y)O_{1-y/2}$ layer to an oxygen chemical potential gradient resulted in its demixing, with the dissolution of the Al^{3+} into the rutile at a lower oxygen partial pressure and its precipitation as Al_2O_3 at a higher partial pressure. When the demixing occurred extensively, the resulting microstructure became highly striated, consisting of three layers, an Al_2O_3-rich layer, an $(Ti_{1-y}Al_y)O_{1-y/2}$-rich layer, and a porous layer, which repeated numerous times[8]. The C atoms were presumed to diffuse through the reaction layers and oxidize. The rate-limiting step was thought to be the diffusion of oxygen and/or Ti[8]. Wang and Zhou studied Ti_3AlC_2 oxidation behavior at 1273–1673 K in air for exposure times up to 20h[11]. The results indicated that Ti_3AlC_2 oxidized following parabolic kinetics, and its excellent oxidation resistance was attributed to the formation of an adherent, continuous inner Al_2O_3 layer, which formed below an outer TiO_2 layer. It is proposed that the inner Al_2O_3 layer might has been formed by the inward diffusion of oxygen through the outer TiO_2 layer, and the outer TiO_2 layer by the outward diffusion of Ti. In 2006, Lee and Park[19b] reported that the oxidation kinetics can lead either to the predominant formation of TiO_2 layers or to the predominant formation of α-Al_2O_3 layers. Needless to add, the samples that formed an Al_2O_3 layer were quite oxidation resistant. In such a case, an inner, thick Al_2O_3 barrier layer formed below the outer, thin TiO_2 layer[11,15,17,19b]. However, when the oxide layers formed were TiO_2-based, the resulting oxidation resistance

was poor. In such a case, either alternating (thick TiO_2 layer)/(thin Al_2O_3 layers) or a thin, intermediate Al_2O_3 barrier layer plus a thick, (TiO_2+Al_2O_3)-mixed layer formed[14,15,19b]. In all cases, the outermost scale is consistently composed of TiO_2[14,15,19b]. It has been demonstrated that the thin Al_2O_3 layer forms first due to the fast diffusion of Al in the basal plane of the MAX phase[19b-19e]. The TiO_2 layers that forms on top of the Al_2O_3 layer results from an outward diffusion of Ti atoms through the grain boundary of preformed Al_2O_3[19b,19d]. Finally, the (TiO_2+Al_2O_3)-mixed layer results from an inward diffusion of oxygen[19b].

In this context, the present study takes the advantage of the comparison of Ti_3AlC_2 and $Ti_3Al_{0.8}Sn_{0.2}C_2$ solid solution synthesized by SPS in order to better understand the role of Sn substitution on A sites on oxidation properties. Hence, oxidation products, kinetics and resistance of the Ti_3AlC_2 and $Ti_3Al_{0.8}Sn_{0.2}C_2$ compounds are compared to finally conclude on the influence of the Al substitution by Sn on the oxidation resistance of 312 MAX phases.

II- Experimental procedures

Ti_3AlC_2 samples were synthesized by powder metallurgy. Titanium, aluminum and titanium carbide powders were blended in quasi stoichiometric proportions (i.e. 1.9TiC-1.05Al-Ti) for 20 min in a Turbula® mixer. The reactant powder mixture is encapsulated in a glass container in vacuum and thus, sintered in argon atmosphere for 2h at 1450°C to produce porous Ti_3AlC_2 bulk material which is subsequently crushed into powder. After the Ti_3AlC_2 synthesis, XRD analysis was systematically performed; the corresponding X-Ray diffractograms (not shown) do not show any impurity at the X-Ray scale. The same is true for the $Ti_3Al_{0.8}Sn_{0.2}C_2$ commercial solid solution provided by Jinghe Technology Co., Ltd. Beijing. For comparison, this in-house Ti_3AlC_2 powder and a commercial $Ti_3Al_{0.8}Sn_{0.2}C_2$ batch were densified by Spark Plasma Sintering (SPS, model HPD 125 FCT system installed in a "Flash Sintering platform" within the University of Burgundy) in vacuum at 1315°C for 2 min at a pressure of 75 MPa with a cooling rate adjusted to 70°C/min. The sample diameters were 60 mm.

X-Ray Diffraction (XRD) analyses were performed using a Bruker D501 diffractometer with Cu-Kα radiation in order to identify the impurities contained in bulk materials and also to identify the oxidation products. XRD data were refined using the MAUD software in order to extract the composition of the different Ti_3AlC_2 and $Ti_3Al_{0.8}Sn_{0.2}C_2$ samples[35]. After an appropriate mechanical polishing of the SPSed samples, Polarized Light Microscopy method (PLM, Zeiss Imager Vario Z2) was used to investigate the grain size distribution and to quantify the amount of the different impurities. The porosity content was measured using the Archimedes method.

The microstructure of the Ti_3AlC_2 and $Ti_3Al_{0.8}Sn_{0.2}C_2$ bulk samples (grain size, distribution of porosity, location and composition of secondary phases) and the one of the oxidation products (morphology and composition of the oxide scale) were examined by Scanning Electron Microscopy using a high resolution field-emission gun scanning electron

microscope (FESEM, Jeol 7001F-TTLS) coupled with energy-dispersive X-ray spectrometer (EDXS, Oxford Energy) for chemical analyses.

Cylindrical (diameter: 6-10mm, thickness: 0.5-2mm) and parallelepiped (2.5x2.5x3 mm^3) specimens were polished with SiC paper up to 2400 grade prior to oxidation tests. Oxidation tests were performed under isothermal conditions over the temperature range 800-1000°C. The oxidation kinetics of Ti_3AlC_2 and $Ti_3Al_{0.8}Sn_{0.2}C_2$ MAX phase compounds were measured using isothermal thermogravimetric tests (Setaram Setsys TG16 and Setaram Setsys Evolution) under synthetic dry air for 30 to 100h. Heating and cooling were performed in argon atmosphere.

III – Results and discussion

III-1- Ti_3AlC_2 and $Ti_3Al_{0.8}Sn_{0.2}C_2$ microstructural characterization

Figure 1 shows the XRD patterns obtained on the Ti_3AlC_2 and $Ti_3Al_{0.8}Sn_{0.2}C_2$ bulk samples. Rietveld refinement of the XRD data underlines the presence of about 0.1-0.2 wt. % of titanium carbide in the sintered samples. As shown in figure 1, the X-ray peaks of the solid solution are displaced to smaller angles reflecting an increase of the cell parameters. Rietveld refinement allows determining the cell parameters (a=3.0747(6) Å and c=18.5720(5) Å) and (a=3.0841(6) Å and c=18.5865(5) Å) of the Ti_3AlC_2 and $Ti_3Al_{0.8}Sn_{0.2}C_2$ compounds respectively. The cell parameters of Ti_3AlC_2 and of $Ti_3Al_{0.8}Sn_{0.2}C_2$ are in very good agreement with the ones published previously[20, 33b, 33d, 33e].

Figure 2 shows back-scaterred SEM micrographs obtained on the Ti_3AlC_2 and $Ti_3Al_{0.8}Sn_{0.2}C_2$ SPSed samples. Figure 2 and EDXS analyses allow demonstrating the presence of small amount of Ti_xAl_y intermetallics (variable x and y contents) and Al_2O_3 grains randomly distributed at Ti_3AlC_2 and $Ti_3Al_{0.8}Sn_{0.2}C_2$ grain boundaries. EDXS analyses enable to confirm the presence of TiC. Al_2O_3 and Ti_xAl_y impurities are either formed during the powder synthesis

or during the densification by SPS. However, TiC is very likely formed during the SPS densification as its presence was not detected by XRD after the powder synthesis. As Al_2O_3 displays rather weak XRD lines and as some of the alumina may be amorphous, this alumina phase is not detected using XRD although the amount of Al_2O_3 is in the same range as the one of TiC. In the same vein, Ti_xAl_y may not be detected as a consequence of the large composition range of the formed Ti_xAl_y and also as a result of the superimposition of the main Ti_xAl_y peaks with the ones of the MAX phase. Using the light microscopy protocol, one can notice that:

- The amount of pores is about the same for both materials (in the range 1-2 vol.% in Ti_3AlC_2 and 1-3 vol.% in $Ti_3Al_{0.8}Sn_{0.2}C_2$)
- The amount of Al_2O_3 is slightly larger in Ti_3AlC_2 (in the range 1.2-1.4 vol.%) compared to $Ti_3Al_{0.8}Sn_{0.2}C_2$ (in the range 0-1.3 vol.%).
- The amount of Ti_xAl_y intermetallics is slightly larger in $Ti_3Al_{0.8}Sn_{0.2}C_2$ (in the range 1-5 vol.%) compared to Ti_3AlC_2 (0.2-1 vol.%).
- The grain size, as determined from the PLM method and from Electron Backscattered Diffraction, is 4.4 µm for the $Ti_3Al_{0.8}Sn_{0.2}C_2$ grains and 3.9 µm for the Ti_3AlC_2 ones (mean equivalent diameter).

III-2- Oxidation behaviors

Figure 3 shows the weight gain per surface area recorded as a function of the oxidation time and at different temperatures on the Ti_3AlC_2 and on the $Ti_3Al_{0.8}Sn_{0.2}C_2$ solid solution. One can notice that the weight gain is very high for the $Ti_3Al_{0.8}Sn_{0.2}C_2$ solid solution compared to the one obtained for Ti_3AlC_2. As an example, it is about 3 $g.m^{-2}$ for Ti_3AlC_2 after 30h at 1000°C and around 300 $g.m^{-2}$ for the solid solution.

After a transient stage, the oxidation kinetics, $\Delta m/A=f(t)$, can be described either by a parabolic or by a cubic law as shown for the Ti_3AlC_2 SPSed samples in figure 4. It has to be noticed that M. W. Barsoum et al. and J. L. Smialek have shown that a cubic law better fits the experimental

results than a parabolic one[15,16]. It thus makes more sense to assume the kinetics to be cubic. Nevertheless, in order to compare our results with other published results on more conventional alloys, a parabolic law was chosen to evaluate corresponding parabolic rate constants (k_p). The obtained values of the parabolic rate constant are given at different temperatures for Ti_3AlC_2 and $Ti_3Al_{0.8}Sn_{0.2}C_2$ in table 1. A comparison of the oxidation kinetics of Ti_3AlC_2 and $Ti_3Al_{0.8}Sn_{0.2}C_2$ shows that the parabolic rate constants of $Ti_3Al_{0.8}Sn_{0.2}C_2$ are, at the same temperatures, 2–4 orders of magnitude greater than those of Ti_3AlC_2. Such a result demonstrates that Ti_3AlC_2 has better oxidation resistance than $Ti_3Al_{0.8}Sn_{0.2}C_2$. Figure 5 shows the Arrhenius plot of k_p versus the inverse of temperature. For both materials, a linear fit is obtained. The slope of the straight line allows calculating the apparent activation energies which are 69 and 336 kJ.mol^{-1} for Ti_3AlC_2 and $Ti_3Al_{0.8}Sn_{0.2}C_2$ respectively. Such a slope can be referred to a true activation energy only in cases where the rate-controlling step is well defined, unique and controlled by diff usion through the oxide scale. It may be the case for the fine-grained Ti_3AlC_2 where Al_2O_3 is the main formed oxide (see figure 8b and 9) however, it is unlikely the case for the solid solution. Thus, the slope of the straight line refers to an apparent activation energy. The apparent activation energy determined for the fine-grained Ti_3AlC_2 sample is smaller than the ones that have been published previously (in the range 136-258 kJ.mol^{-1})[11,17,18]. Thus, the apparent activation energy that is obtained for our fine-grained Ti_3AlC_2 specimens (69 kJ.mol^{-1}) implies that the first stages of oxidation, which allows alumina formation, is easier than the ones implied for fine-grained $Ti_3Al_{0.8}Sn_{0.2}C_2$. One has also to notice that the parabolic rate constants are less temperature dependent for the former specimens.

Figure 6 shows a cross-section view of the oxide layer observed by SEM on the Ti_3AlC_2 SPSed specimen oxidized during 1000h at 1000°C. Ti, Al, C and O corresponding EDXS maps of the oxide layer are once more presented. After 1000h of oxidation, the thickness of the oxide layer, mainly composed of Al_2O_3, is about 3 µm. Some nodules of TiO_2 are observed on top of

the Al_2O_3 layer. Such a microstructure of the oxide scale has been observed in a lot of works[11,12,15,19c,19d,19e] and is characteristic of a Ti_3AlC_2 with a good oxidation resistance[15]. The Al_2O_3 layer effectively inhibited the oxidation, the scale being dense and adherent; carbon is not detected in the oxide layer. As demonstrated by Rao et al.[19e], α-Al_2O_3 nuclei nucleate on the Ti_3AlC_2 matrix and grow in the initial stage of oxidation, forming the inner Al_2O_3 oxide scale. Once the depletion of Al atoms occurs in the surface layer of Ti_2AlC matrix, Ti atoms start to diffuse out and form the outer TiO_2 layer.

Figure 7a and 7b show a cross-section view of the oxide layer observed by SEM on the Ti_3AlC_2 SPSed specimen oxidized for 24h (a) and 500h (b) at 800°C. Ti, Al, C and O corresponding EDXS maps of the oxide layer are also presented. After 24h of oxidation, the thickness of the oxide layer is about 7 µm, on top of the Ti_3AlC_2 phase, the oxide layer consists in a mixture of Al_2O_3 and TiO_2. After 500h of oxidation, the thickness of the oxide layer is about 20 µm, the layer in contact with the Ti_3AlC_2 phase consists in a mixture of Al_2O_3 and TiO_2, the intermediate layer consists in Al_2O_3 and the external layer mainly consists in TiO_2. One can also notice that carbon is very likeley present inside the oxide scale. Such a microstructure of the oxide scale has been observed and discussed by Lee and Park[19b]. The authors have shown, using Pt marker on the Ti_3AlC_2 surface, that Al_2O_3 thin layer is primarily formed and that TiO_2 nodules are formed on top of the Al_2O_3 thin layer by outward diffusion of Ti^{4+}. Song et al.[19d], noticing that the amount of TiO_2 after 0.5 and 80 h oxidation remains the same, suggest that the TiO_2 nodule formation is terminated once a dense and continuous Al_2O_3 layer is formed. Lee and park[19b] demonstrated that the mixed (Al_2O_3+TiO_2) layer results from the internal oxidation of Ti_3AlC_2 down to the thin Al_2O_3 layer ; it is formed due to inward diffusion of O^{2-} when the alumina scale is not dense enough.

Figure 8 shows a cross-section of the oxide layer observed by SEM on the $Ti_3Al_{0.8}Sn_{0.2}C_2$ SPSed specimen oxidized for 30h at 850°C, simultaneously with Ti, Al, C, O and Sn corresponding EDXS maps of the oxide layer. The oxide thickness is about 30 μm. It consists in six layers: the first one, adjacent to the MAX phase, is a mixture of TiO_2 and Al_2O_3, the second one consits in a tin oxide whose stoechiometry has not been determined due to the proximity of the other oxides (it is nevertheless quite reasonable to assume that the tin oxide consists in SnO_2), the third layer is also a mixture of TiO_2 and Al_2O_3, the fourth one is a tin oxide, the fifth one is Al_2O_3 and finally the last one consists in TiO_2. Some pores are observed inside the oxide scale, mainly at the interface between the external TiO_2 layer and the Al_2O_3 adjacent layer. It is now well known that, during the oxidation of Ti_3AlC_2 and Ti_2AlC MAX phases, a protective α-Al_2O_3 layer forms first followed by a discontinuous TiO_2 layer formed on top after long time of oxidation[19b,19d,19e]. The lower bond-breaking energy of Al–Ti bonds in the MAX phase is the driving force of this preferential oxidation process. During the oxidation of the $Ti_3Al_{0.8}Sn_{0.2}C_2$ solid solution, it is possible that a SnO_2 layer forms first. Indeed, *ab initio* calculations of the Al–Sn substitution predict a cohesive energy reduction of 21.7% which is supposed to contribute to a reduction in the thermal stability and to an easier mobility of Sn compared to Al in the A planes of the MAX[36]. Once a first SnO_2 layer is formed, a continuous α-Al_2O_3 layer forms followed by the formation of the discontinuous TiO_2 upper layer. Due to the inward diffusion of oxygen through the grain boundary, the internal oxidation of the solid solution can continue and lead to the multilayered microstructure shown in figure 8.

After oxidation at 950°C for 30h, the same oxides are formed as shown in figure 9. The Al_2O_3 and TiO_2 external layers are mixed at this temperature to form a single layer consisting in a crystallite's mixture of the two oxides. Moreover, the adhesion of the oxide layer seems to be poorer than the one formed at 850°C; the external TiO_2, Al_2O_3 and SnO_2 layers are scaled (see

red arrow in figure 9) whereas microcracks and debonding are observed in the oxide layer and also at the interface between the 312 phase and the oxide layer (see blue arrow in figure 9).

Oxidation tests performed on $Ti_3Al_{0.8}Sn_{0.2}C_2$ solid solution demonstrate the harmful effect of Al substitution by Sn atoms. Although the tin oxide formation is thermodynamically less favourable than the Al_2O_3 or TiO_2 ones, the atomic position of tin atoms in the hexagonal structure of the MAX phase (in the A planes) and the weak M-A bonds lead to an easy outward diffusion of Sn (and Al) atoms to the interfaces (oxide/air, MAX/oxide). Moreover, a quite large amount of non protective rutile TiO_2 is formed on the surface of the $Ti_3Al_{0.8}Sn_{0.2}C_2$ solid solution. Such a deleterious TiO_2 formation likely results from the Al/Ti atom's ratio, about 0.27 in this case, which is far from 0.32. Indeed, Li et al. have shown that, for Al/Ti atom's ratio smaller than 0.32, aluminum atom supply at the MAX phase/oxide interface is insufficient to inhibit TiO_2 growth[19].

IV- Summary

Highly pure (secondary phases in the range 2-5 weight %) and dense (porosity smaller than 2 vol.%) Ti_3AlC_2 and $Ti_3Al_{0.8}Sn_{0.2}C_2$ bulk samples have been synthesized by coupling natural sintering and SPS densification. The PLM method demonstrates that grain size is small (mean equivalent diameters are smaller than 5 μm). Finally, oxidation tests were performed on the Ti_3AlC_2 compound and on the $Ti_3Al_{0.8}Sn_{0.2}C_2$ solid solution. It is demonstrated that the substitution of Al atoms by Sn atoms in the A plane of the MAX phase has a harmful effect on the oxidation resistance. Indeed, the oxidation kinetics is very high for the solid solution compared to the one of the Ti_3AlC_2 compound (parabolic rate constant is 3 order of magnitude smaller in the case of Ti_3AlC_2). The presence of Sn atoms in the A planes of the solid solution leads to an easy diffusion of Sn atoms out of the MAX phase. As a result, tin oxide, a non-

protective oxide, is formed. Moreover, Al/Ti atom's ratio being small, non-protective rutile-TiO_2 is also formed. The oxide layer, on top of the $Ti_3Al_{0.8}Sn_{0.2}C_2$ solid solution thus consists in TiO_2, SnO_2 and Al_2O_3. On the opposite, the oxide layer formed on top of the Ti_3AlC_2 phase mainly consists in a protective Al_2O_3 layer; a few TiO_2 grains being observed on top of this oxide layer.

Acknowledgements:

The authors acknowledge SAFRAN for the financial support and for E. Drouelle PhD grant.

References

[1]M. W. Barsoum, "The $M_{N+1}AX_N$ phases: A new class of solids thermodynamically stable nanolaminates," *Progress in Solid State Chemistry,* **28**[1-4] 201-81(2000).

[2]W. Jeitschko, H. Nowotny and F. Benesovsky, "Kohlen-stoffhaltige ternare Verbindungen (H-Phase)," *Monatshefte für Chemie,* **94**[4] 672-76(1963).

[3]W. Jeitschko, H. Nowotny and F. Benesovsky, "Die H-phasen Ti_2TlC, Ti_2PbC, Nb_2InC, Nb_2SnC und Ta_2GaC," *Monatshefte für Chemie,* **95**[2] 431-35 (1964).

[4]W. Jeitschko and H. Nowotny, "Die Kristallstructur von Ti_3SiC_2-Ein Neuer Komplxcarbid-Typ," *Monatshefte für Chemie,* **98**[2] 329-37(1967).

[5]M.W. Barsoum, T. El-Raghy, Synthesis and characterization of a remarkable ceramic: Ti_3SiC_2, J. Am. Ceram. Soc., 79 (1996) 1953–1956.

[6]M.W. Barsoum, The $M_{n+1}AX_n$ Phases : A New Class of Solids, Prog. Solid State Chem. 28 (2000) 201–281.

[7]M.W. Barsoum, MAX Phases: Properties of Machinable Ternary Carbides and Nitrides, in: Wiley VCH, Weinheim, 2013.

[8]N. V. Tzenov and M. W. Barsoum, "Synthesis and characterization of Ti_3AlC_2," *Journal of the American Ceramic Society,* **83**[4] 825-32 (2000).

[9]X. H. Wang and Y. C. Zhou, "Microstructure and properties of Ti_3AlC_2 prepared by the solid-liquid reaction synthesis and simultaneous in-situ hot pressing process," *Acta Materialia,* **50**[12] 3141-49 (2002).

[10]H. Zhai, Z. Huang, M. Ai, Y. Zhou, Z. Zhang and S. Li, "Tribophysical properties of polycrystalline bulk Ti_3AlC_2," *Journal of the American Ceramic Society,* **88**[11] 3270-74 (2005).

[11]X. H. Wang and Y. C. Zhou, "Oxidation behavior of Ti_3AlC_2 at 1000-1400°C in air," *Corrosion Science,* **45**[5] 891-907 (2003).

[12]X. H. Wang and Y. C. Zhou, "High-temperature oxidation behavior of Ti_2AlC in air," *Oxidation of Metals,* **59**[3-4] 303-20 (2003).

[13]M. Sundberg, G. Malmqvist, A. Magnusson and T. El-Raghy, "Alumina forming high temperature silicides and carbides," *Ceramics International,* **30**[7] 1899-904 (2004).

[14]M. W. Barsoum, N. Tzenov, A. Procopio, T. El-Raghy and M. Ali, Oxidation of $Ti_{n+1}AlX_n$ (n = 1 - 3 and X = C , N): II. Experimental Results, *J. Electrochem. Soc.* 148 (8), 2001, 551-562.

[15]D. J. Tallman , B. Anasori and M. W. Barsoum, A Critical Review of the Oxidation of Ti_2AlC, Ti_3AlC_2 and Cr_2AlC in Air, *Materials Research Letters*, 1, 3 (2013) 115-125.

[16]J. L. Smialek, Kinetic Aspects of Ti_2AlC MAX Phase Oxidation, *Oxidation of Metals*, 83, 3–4 (2015) 351-366.

[17]X. W. Xu, Y. Li, B. C. Mei, J. Q. Zhu, H. Liu, and J. Qu, “Study on the Isothermal Oxidation Behavior in Air of Ti_3AlC_2 Sintered by Hot Pressing.” *Science in China Series E: Technological Sciences* 49 (5), 2006, 513–20.

[18]X. H. Wang and Y. C. Zhou, “Oxidation Behavior of TiC-Containing Ti_3AlC_2 Based Material at 500-900 °C in Air.” *Materials Research Innovations* 7(6), 2003, 381–90.

[19]X. C. Li, Y. H. Qian, L. Zheng, J. J. Xu, and M. S. Li, “Determination of the Critical Content

of Al for Selective Oxidation of Ti_3AlC_2 at 1100°C." *Journal of the European Ceramic Society* 36 (14) 2016, 3311-3318.

[19b]D. B. Lee, S. W. Park, "High-temperature oxidation of Ti_3AlC_2 between 1173 and 1473 K in air. ", *Mater. Sci. Eng A.* 434 (2006) 147–154.

[19c]H. J. Yang, Y. T. Pei, J. C. Rao, J. Th. M. De Hosson, S. B. Li and G. M. Song, "High temperature healing of Ti_2AlC: On the origin of inhomogeneous oxide scale", Scripta Materialia 65 (2011) 135–138.

[19d]G. M. Song, V. Schnabel, C. Kwakernaak, S. van der Zwaag, J. M. Schneider and W. G. Sloof, "High temperature oxidation behaviour of Ti_2AlC ceramic at 1200°C », Materials at high temperatures, 29, 3 (2012) 205-209.

[19e]J. C. Rao, Y. T. Pei, H. J. Yang, G. M. Song, S.B. Li, J. Th. M. De Hosson, TEM study of the initial oxide scales of Ti_2AlC, Acta Materialia 59 (2011) 5216–5223.

[20]M. A. Pietzka and J. C. Schuster, "Summary of constitutional data on the Aluminum-Carbon-Titanium system.", *Journal of Phase Equilibria,* **15**[4] (1994) 392-400.

[21]X. Wang and Y. Zhou, "Solid-liquid reaction synthesis of layered machinable Ti_3AlC_2 ceramic," *Journal of Materials Chemistry,* **12**[3] (2002) 455-60.

[22]A.G. Zhou, C.A. Wang, Y. Huang, "Synthesis and mechanical properties of Ti_3AlC_2 by spark Plasma Sintering", J. Mater. Sci., 38 (2003) 3111.

[23]J.Q. Zhu, B.C. Mei, X.W. Xu, J. Liu, “Synthesis of single-phase polycrystalline Ti_3SiC_2 and Ti_3AlC_2 by hot pressing with the assistance of metallic Al or Si”, Mater. Lett. 58 (2004) 588-592.

[24]J. H. Han, S. S. Hwang, D. Lee and S. W. Park, "Synthesis and mechanical properties of Ti_3AlC_2 by hot pressing TiC_x/Al powder mixture," *Journal of the European Ceramic Society,* **28**[5] 979-88(2008).

[25]W. Zhou, B. Mei, J. Zhu and X. Hong, "Synthesis of high-purity Ti_3SiC_2 and Ti_3AlC_2 by spark plasma sintering (SPS) technique," *Journal of Materials Science,* **40**[8] 2099-100(2005).

[26]G. Liu, K. Chen, H. Zhou, J. Guo, K. Ren and J. M. F. Ferreira, "Layered growth of Ti_2AlC and Ti_3AlC_2 in combustion synthesis," *Materials Letters,* **61**[3] 779-84(2007).

[27]C. L. Yeh and Y. G. Shen, "Combustion synthesis of Ti_3AlC_2 from Ti/Al/C/TiC powder compacts," *Journal of Alloys and Compounds,* **466**[1-2] 308-13(2008).

[28]C. Peng, C. A. Wang, Y. Song and Y. Huang, "A novel simple method to stably synthesize Ti_3AlC_2 powder with high purity," *Materials Science and Engineering A,* **428**[1-2] 54-58(2006).

[29]S. B. Li, H. X. Zhai, G. P. Bei, Y. Zhou and Z. L. Zhang, "Formation of Ti_3AlC_2 by mechanically induced self-propagating reaction in Ti-Al-C system at room temperature," *Materials Science and Technology,* **22**[6] 667-72(2006).

[30]S. B. Li, H. X. Zhai, G. P. Bei, Y. Zhou and Z. L. Zhang, "Synthesis and microstructure of Ti_3AlC_2 by mechanically activated sintering of elemental powders," *Ceramics International,* **33**[2] 169-73(2007).

[31]J. Zhu, B. Mei, X. Xu and J. Liu, "Synthesis of single-phase polycrystalline Ti_3SiC_2 and Ti_3AlC_2 by hot pressing with the assistance of metallic Al or Si," *Materials Letters*, **58**[5] 588-92(2004).

[32]M. X. Ai, H. X. Zhai, Y. Zhou, Z. Y. Tao, Z. Y. Huang, Z. L. Zhang and S. B. Li, "Synthesis of Ti_3AlC_2 powders using Sn as an additive," *Journal of the American Ceramic Society*, **89**[3] 1114-17(2006).

[33]S. B. Li, W. H. Xiang, H. X. Zhai, Y. Zhou, C. W. Li and Z. L. Zhang, "Formation of a single-phase Ti_3AlC_2 from a mixture of Ti, Al and TiC powders with Sn as an additive," *Materials Research Bulletin*, **43**[8-9] 2092-99(2008).

[33b]G. P. Bei, V. Gauthier-Brunet, C. Tromas and S. Dubois, "Synthesis, characterization and intrinsic hardness of layered nanolaminate Ti_3AlC_2 and $Ti_3Al_{0.8}Sn_{0.2}C_2$ solid solution," J. Am. Ceram. Soc., 95[11] 102-107 (2012).

[33c]S. Dubois, G. P. Bei, C. Tromas, V. Gauthier-Brunet and P. Gadaud, "Synthesis, microstructure, and mechanical properties of $Ti_3Sn_{(1-x)}Al_xC_2$ MAX phase solid solutions," *Inter. J. Appl. Ceram. Tech.*, **7**[6] 719-29(2010).

[33d]Y. C. Zhou, J. C. Chen, J. Y. Wang, “Strengthening of Ti_3AlC_2 by incorporation of Si to form $Ti_3Al_{1-x}Si_xC_2$ solid solutions.”, Acta Materialia 54(5) (2006) 1317-1322.

[33e]X. H. Yin, M. Li, T. P. Li, Y. C. Zhou, “Diffusion Bonding of Ti3AlC2 Ceramic via a Si Interlayer”, Journal of Materials Science 42(17):7081-7085.

[34]C. Peng, C. A. Wang, L. Qi and Y. Huang, "Fabrication of Ti_3AlC_2 powder with high-purity by pressureless sintering," *Materials Science Forum*, **475-479** 1247-50(2005).

[35]L. Lutterotti, S. Matthies, and H.-R. Wenk, MAUD: A Friendly Java Program for Material Analysis using Diffraction, *IUCr: Newsletter CPD*, 21, 1999, 14.

[36]B. Liu, J. Y. Wang, J. Zhang, F. Z. Li, and Y. C. Zhou, "Theoretical Investigation of A-Element Atom Diffusion in Ti2AC (A=Sn, Ga, Cd, In, and Pb)," Appl. Phys. Lett., 94 [18] 181906, 3pp (2009).

Figures captions

Figure 1: XRD patterns obtained on Ti_3AlC_2 and $Ti_3Al_{0.8}Sn_{0.2}C_2$ SPSed samples.

Figure 2: Back-scattered SEM micrographs of (a) Ti_3AlC_2 and (b) $Ti_3Al_{0.8}Sn_{0.2}C_2$ SPSed samples.

Figure 3: Weight gain per surface area unit ($\Delta m/A$) measured as a function of time at different temperatures and for (a) Ti_3AlC_2 and (b) $Ti_3Al_{0.8}Sn_{0.2}C_2$ SPSed samples.

Figure 4: (a) $(\Delta m/A)^2$ and (b) $(\Delta m/A)^3$ versus time. Experimental data have been recorded on a Ti_3AlC_2 SPSed sample.

Figure 5: Arrhenius plot of the parabolic rate constant as a function of the inverse of temperature for the Ti_3AlC_2 (blue squares) and the $Ti_3Al_{0.8}Sn_{0.2}C_2$ solid solution (orange circles) SPSed samples. Experimental results from references 11 (red squares), 17 (orange diamond) and 18 (black circles) are also plotted.

Figure 6: Cross-section view of the oxide layer observed by SEM on the Ti_3AlC_2 SPSed specimen oxidized during 1000h at 1000°C. Ti, Al, C and O corresponding EDXS maps of the oxide scale. A schematic representation of the different oxide's layer is also given.

Figure 7: Cross-section view of the oxide layer observed by SEM on the Ti_3AlC_2 SPSed specimen oxidized during 24h (a) and 500h (b) at 800°C. Ti, Al, C and O corresponding EDXS maps of the oxide scale. A schematic representation of the different oxide's layer is also given.

Figure 8: Cross-section view of the oxide layer observed by SEM on the $Ti_3Al_{0.8}Sn_{0.2}C_2$ SPSed specimen oxidized during 30h at 850°C. Ti, Al, C, O and Sn corresponding EDXS maps of the oxide scale. A schematic representation of the different oxide's layer is also given.

Figure 9: Cross-section view of the oxide layer observed by SEM on the $Ti_3Al_{0.8}Sn_{0.2}C_2$ SPSed specimen oxidized during 30h at 950°C. The red arrow shows that the external TiO_2, Al_2O_3 and SnO_2 layers are scaled whereas the blue arrow shows microcracks and debonding inside the oxide layer.

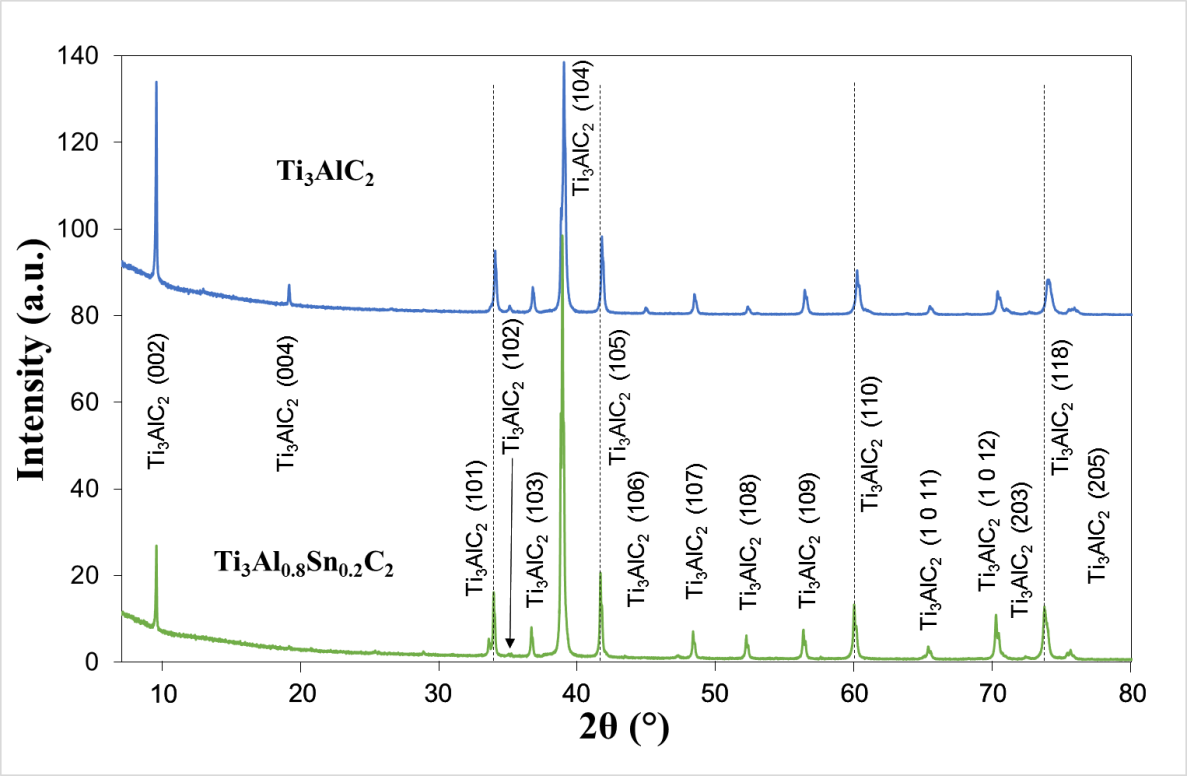

Figure 1: XRD patterns recorded on Ti_3AlC_2 and $Ti_3Al_{0.8}Sn_{0.2}C_2$ SPSed samples.

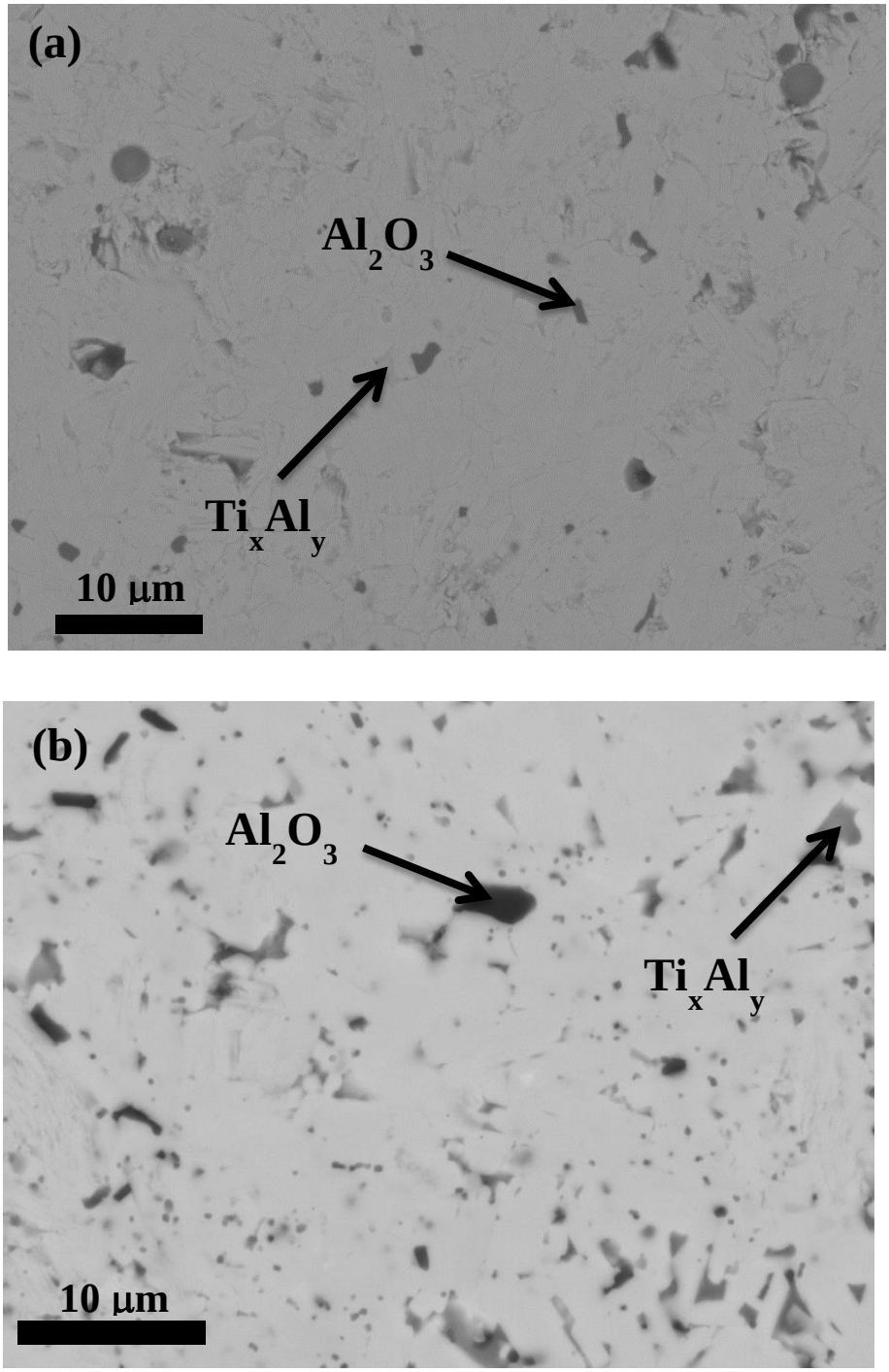

Figure 2: Back-scattered SEM image of (a) Ti_3AlC_2 and (b) $Ti_3Al_{0.8}Sn_{0.2}C_2$ SPSed samples.

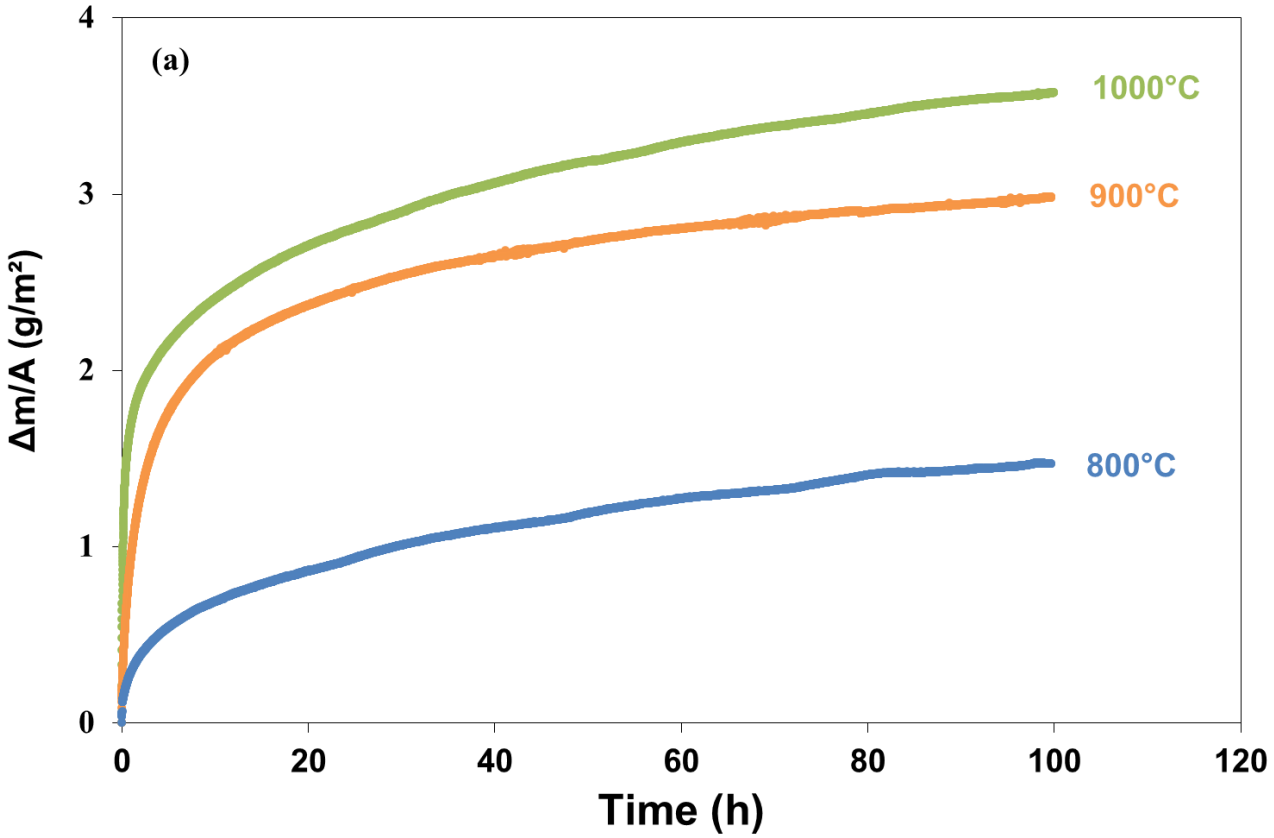
(a)
1000°C
900°C
800°C
Δm/A (g/m²)
Time (h)
0
1
2
3
4
0
20
40
60
80
100
120

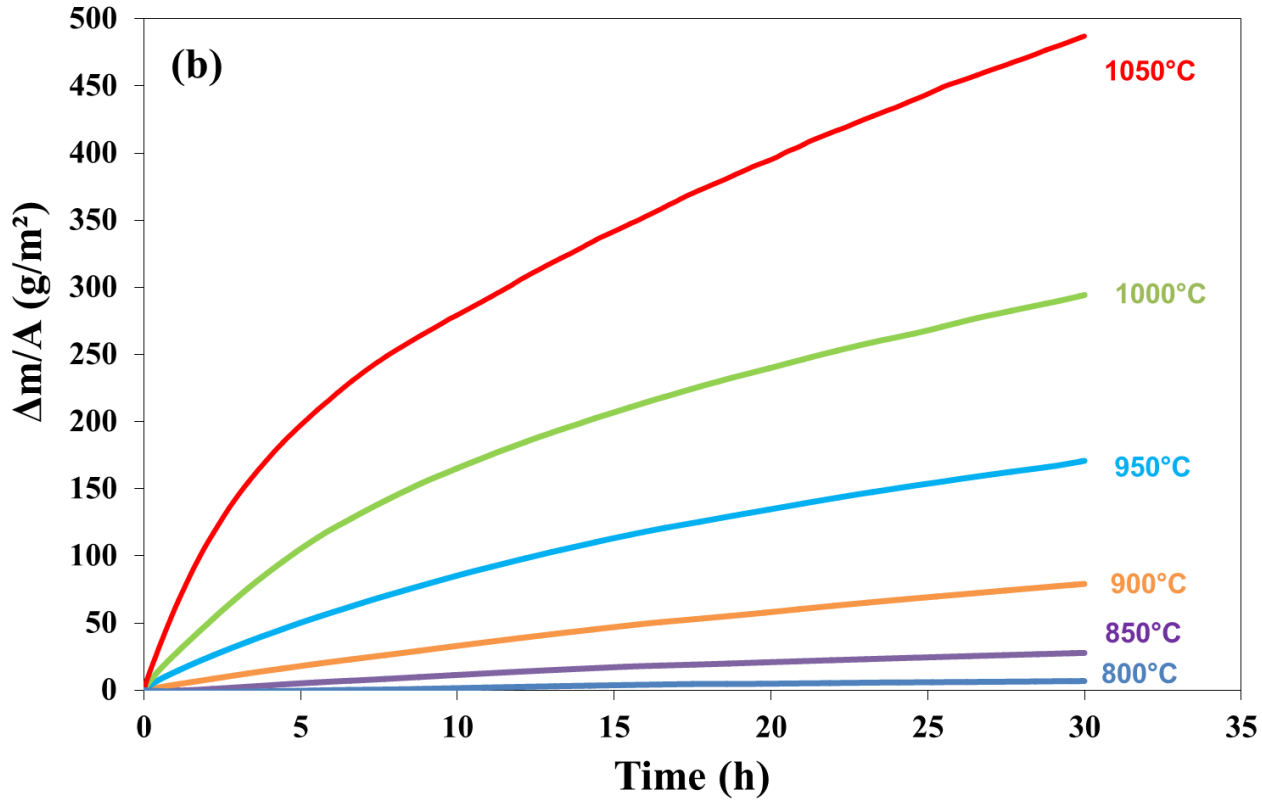
(b)
1050°C
1000°C
950°C
900°C
850°C
800°C
Δm/A (g/m²)
Time (h)
0
50
100
150
200
250
300
350
400
450
500
0
5
10
15
20
25
30
35

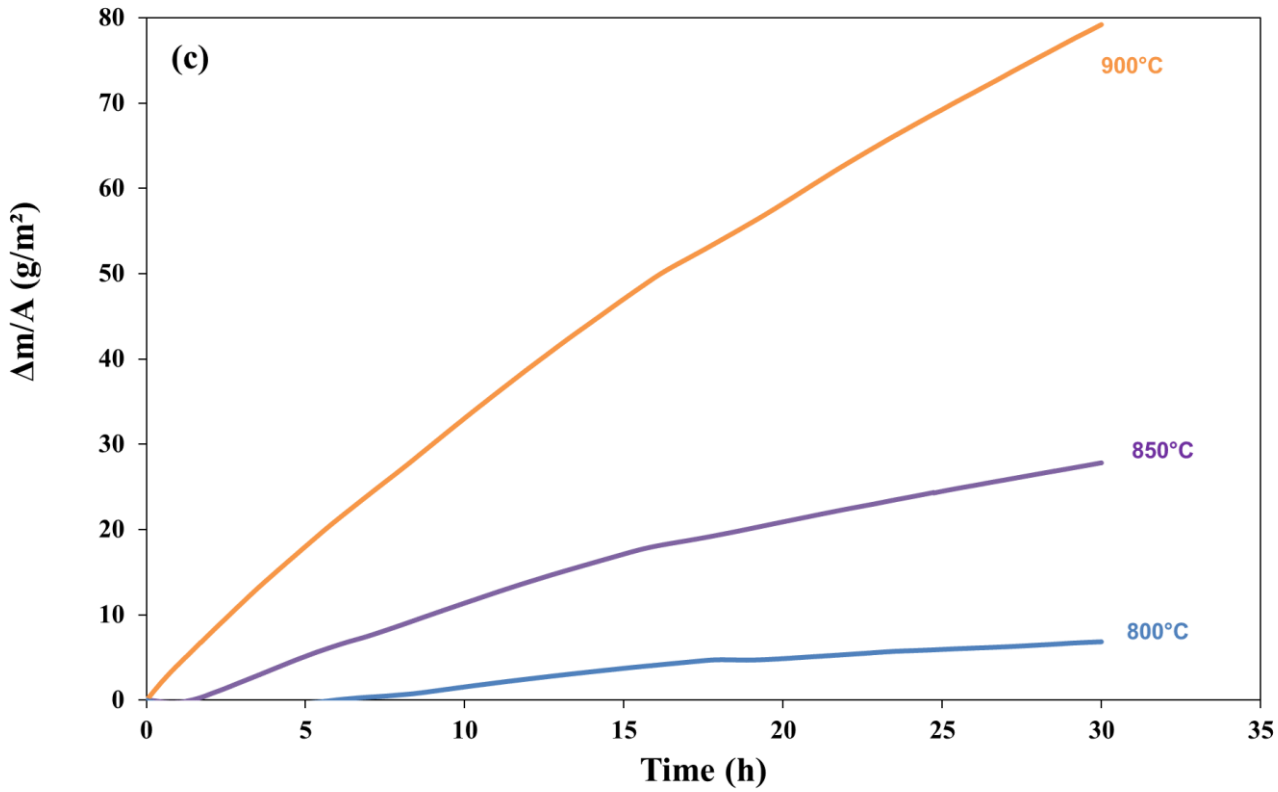

Figure 3: Weight gain per surface area unit (Δm/A) measured as a function of time at different temperatures and for (a) Ti_3AlC_2 and (b) $Ti_3Al_{0.8}Sn_{0.2}C_2$ SPSed samples.

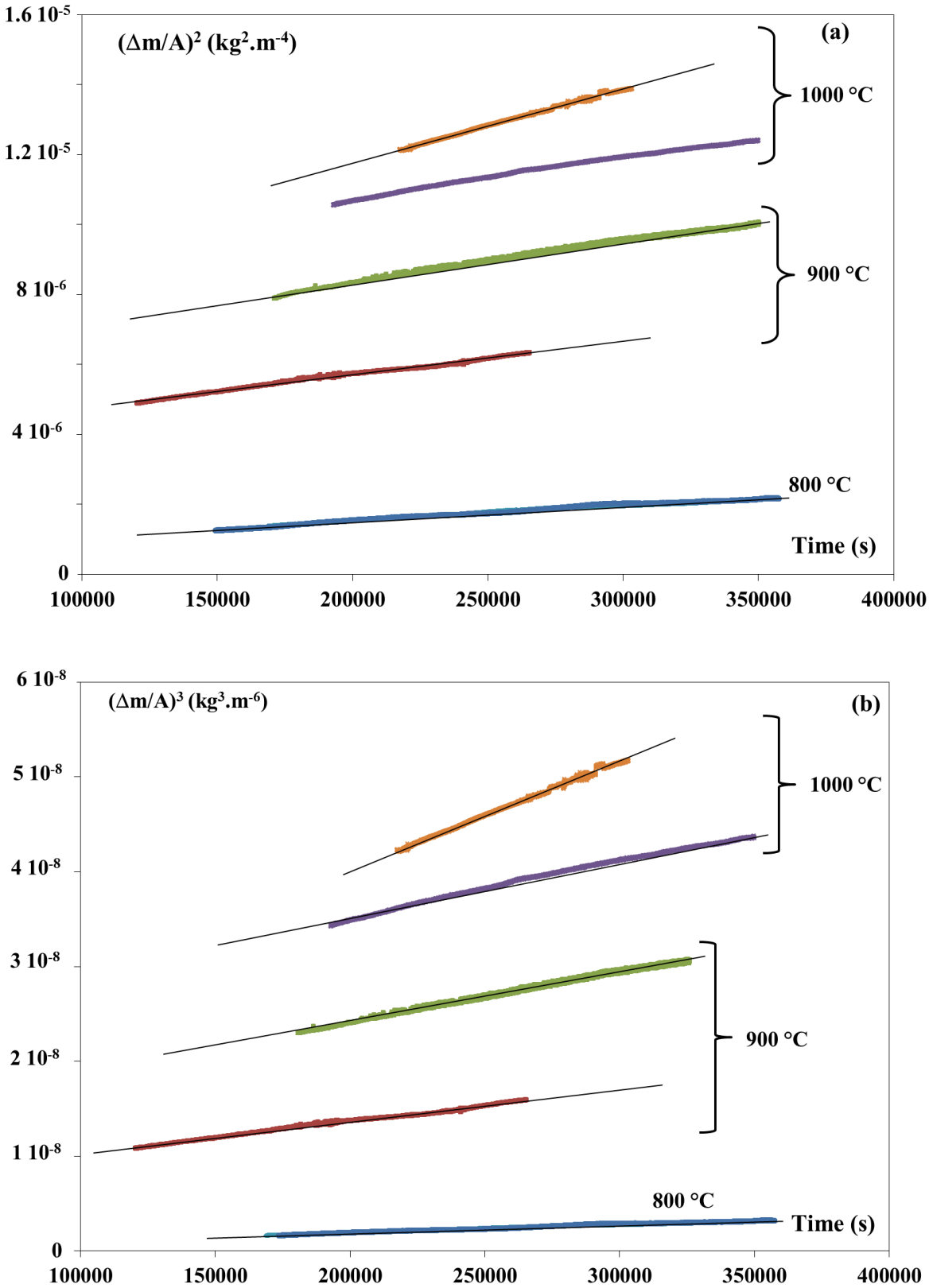

Figure 4: (a) $(\Delta m/A)^2$ and (b) $(\Delta m/A)^3$ versus time. Experimental data have been recorded on a Ti_3AlC_2 SPSed sample.

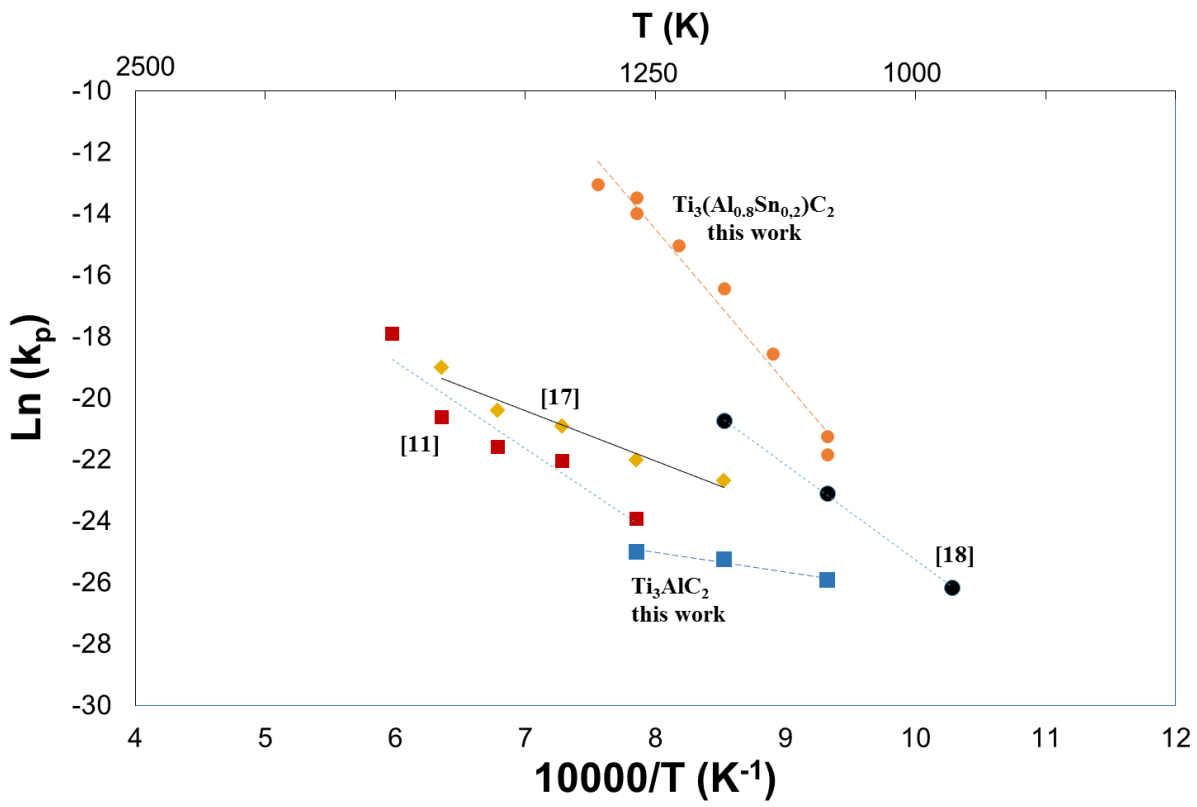

Figure 5: Arrhenius plot of the parabolic rate constant as a function of the inverse of temperature for the Ti_3AlC_2 (blue squares) and the $Ti_3Al_{0.8}Sn_{0.2}C_2$ solid solution (orange circles) SPSed samples. Experimental results from references 11 (red squares), 17 (orange diamond) and 18 (black circles) are also plotted.

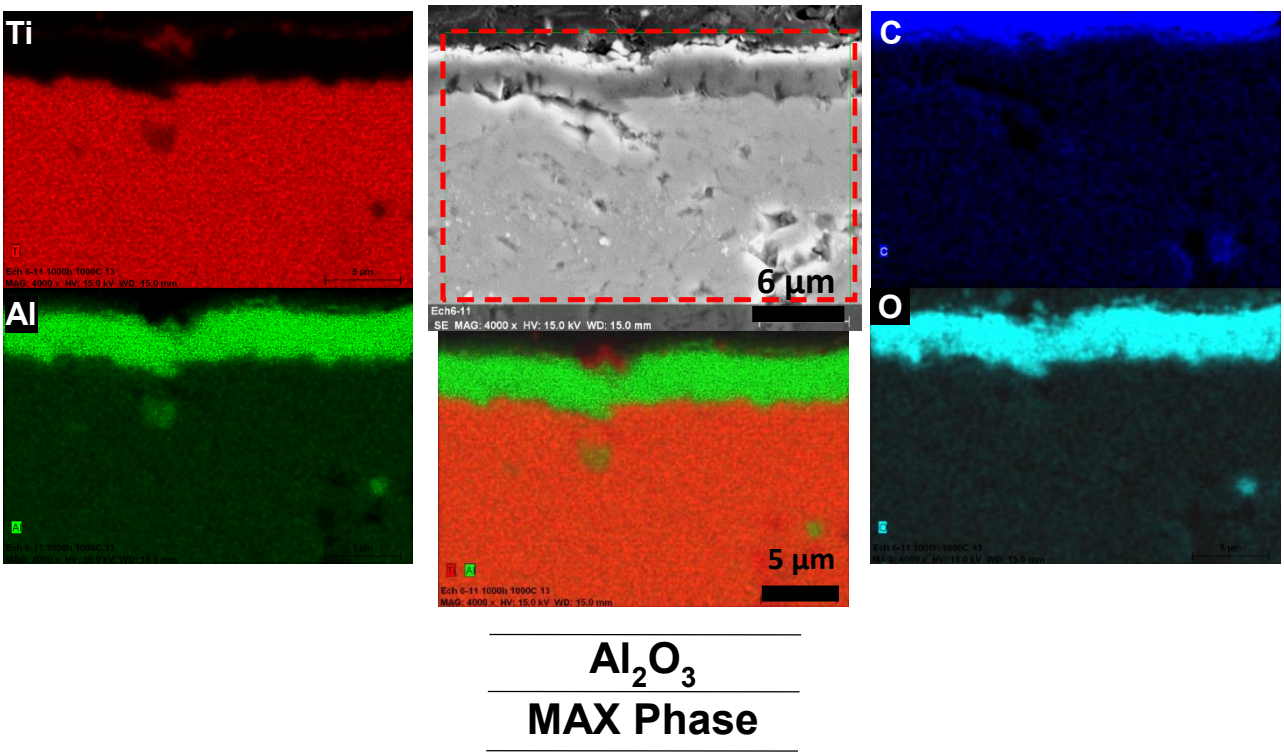

Figure 6 : Cross-section view of the oxide layer observed by SEM on the Ti_3AlC_2 SPSed specimen oxidized during 1000h at 1000°C. Ti, Al, C and O corresponding EDXS maps of the oxide scale. A schematic representation of the different oxide's layer is also given.

(a) 800°C 24h

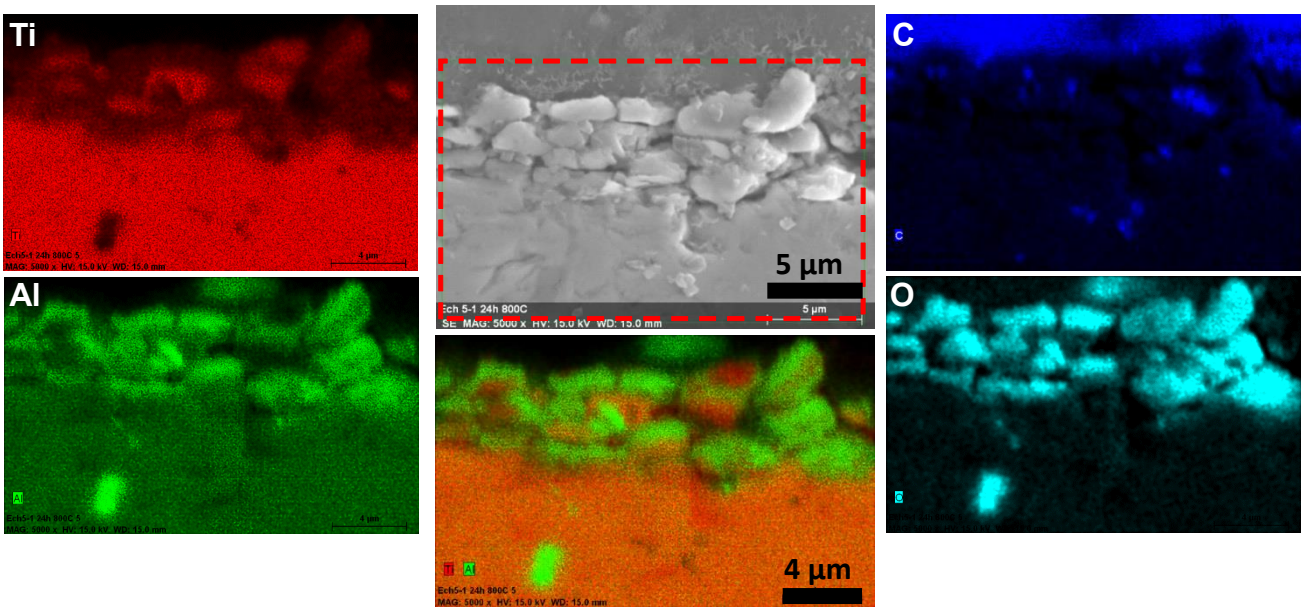

$TiO_2 + Al_2O_3$

MAX Phase

(b) 800°C 500h

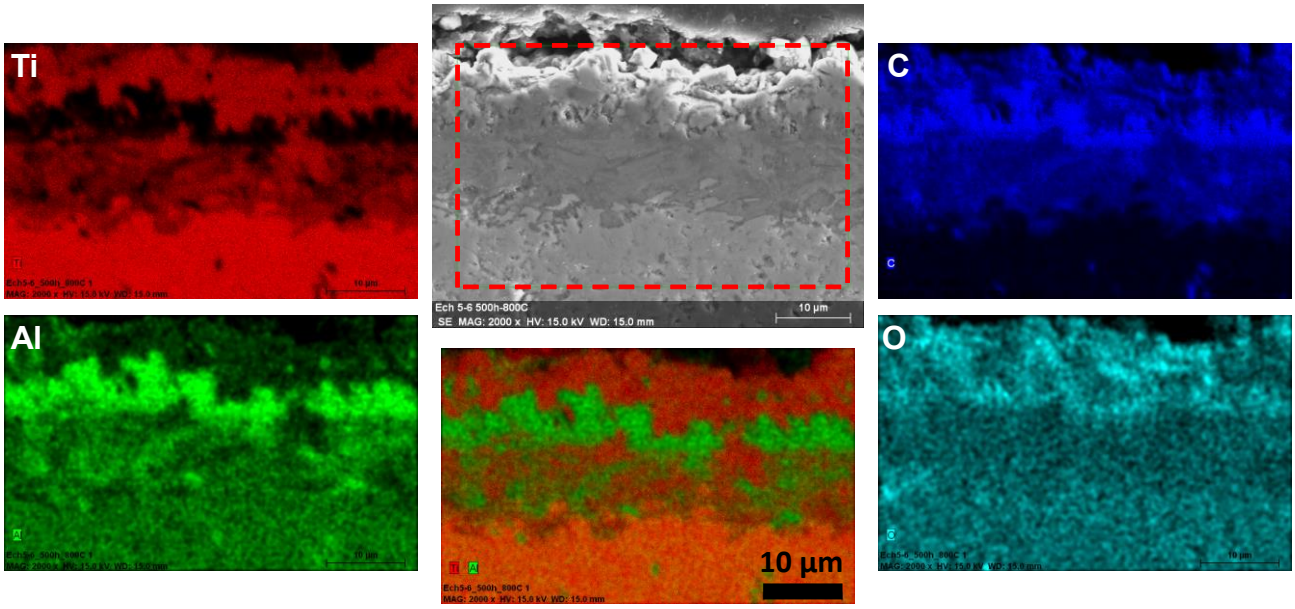

TiO_2

Al_2O_3

$TiO_2 + Al_2O_3$

MAX Phase

Figure 7 : Cross-section view of the oxide layer observed by SEM on the Ti_3AlC_2 SPSed specimen oxidized during 24h (a) and 500h (b) at 800°C. Ti, Al, C and O corresponding EDXS maps of the oxide scale. A schematic representation of the different oxide's layer is also given.

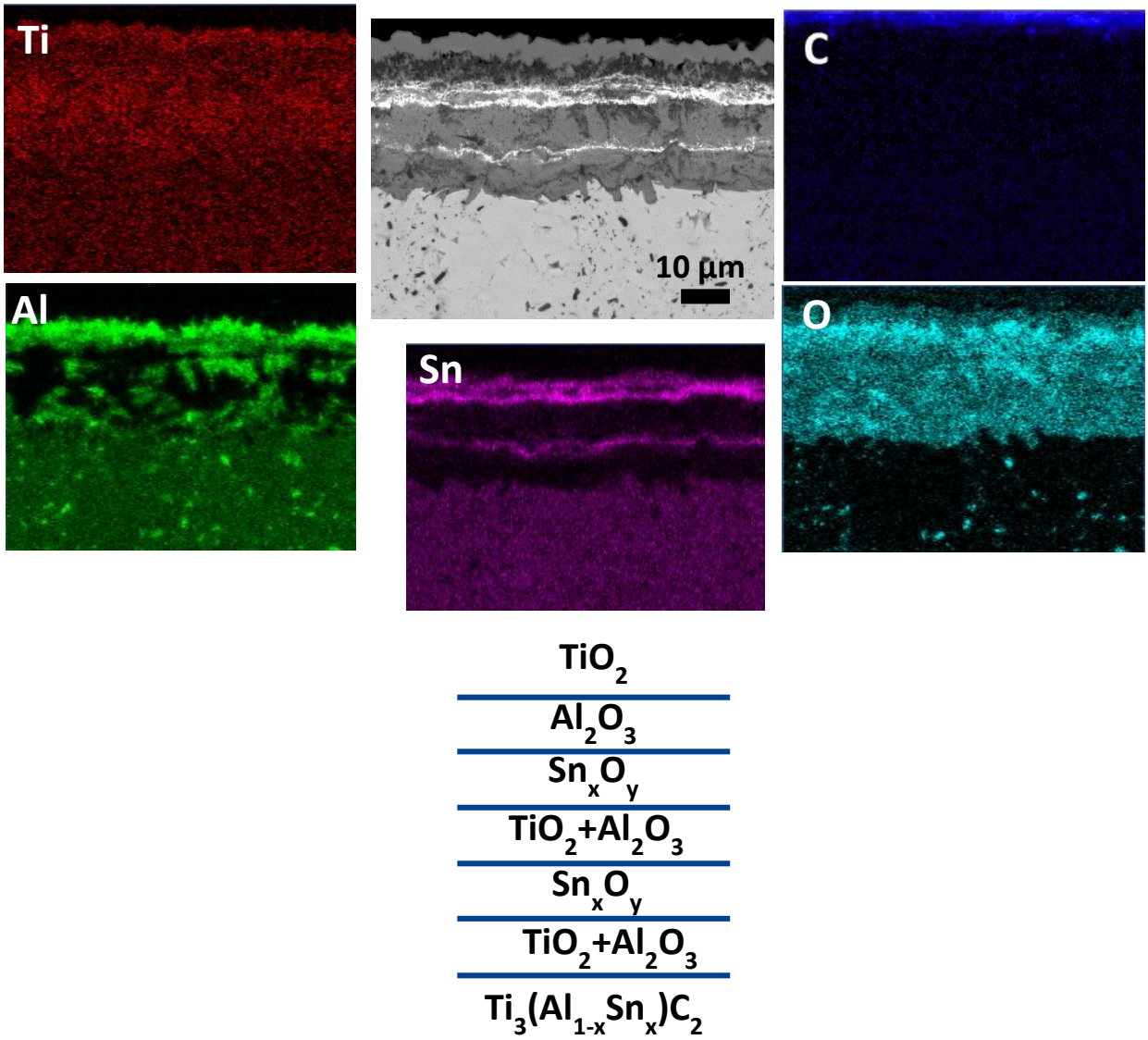

Figure 8: Cross-section view of the oxide layer observed by SEM on the $Ti_3Al_{0.8}Sn_{0.2}C_2$ SPSed specimen oxidized during 30h at 850°C. Ti, Al, C, O and Sn corresponding EDXS maps of the oxide scale. A schematic representation of the different oxide's layer is also given.

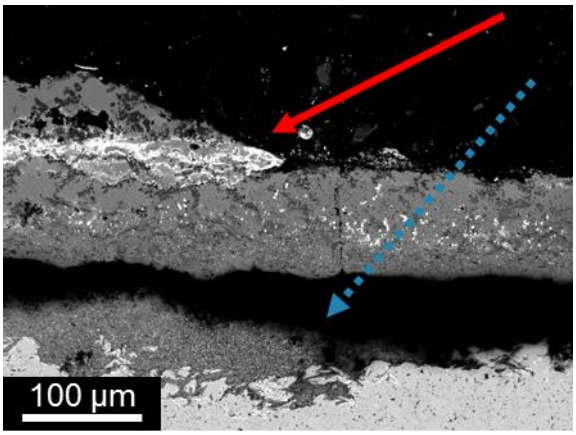

Figure 9: Cross-section view of the oxide layer observed by SEM on the $Ti_3Al_{0.8}Sn_{0.2}C_2$ SPSed specimen oxidized during 30h at 950°C. The red arrow shows that the external TiO_2, Al_2O_3 and SnO_2 layers are scaled whereas the blue arrow shows microcracks and debonding inside the oxide layer.

		800°C	850°C	900°C	950°C	1000°C	1050°C
k_p ($kg^2/m^4/s$)	**$Ti_3(Al_{1-x}Sn_x)C_2$**	**$6{,}0.10^{-10}$**	**$8{,}8.10^{-9}$**	**$7{,}3.10^{-8}$**	**$3{,}0.10^{-7}$**	**$8{,}4.10^{-7}$**	**$2{,}2.10^{-6}$**
	Ti_3AlC_2	**$5{,}6.10^{-12}$**		**$1{,}1.10^{-11}$**		**$1{,}4.10^{-11}$**	

Table 1 : Kinetic rate constant determined at different temperatures on the $Ti_3Al_{0.8}Sn_{0.2}C_2$ and Ti_3AlC_2 MAX phase.